Malaysian Journal of Chemistry, 2023, Vol. 25(3), 202-211
(Special Issue: *Rubbercon2022*)

Formation of Form-Stable Polyamide/Reduced Graphene Oxide Phase Change Material for High Temperature Applications using Nitrile Butadiene Rubber Coating

Patmashini Saii K. Nithyananthan[1], Yamuna Munusamy[1,*], Kok Seng Ong[2]
[1]Department of Petrochemical Engineering, Faculty of Engineering and Green Technology, Universiti Tunku Abdul Rahman, Jalan Universiti, Bandar Barat, Kampar, Perak 31900, Malaysia
[2]Department of Industrial Engineering, Faculty of Engineering and Green Technology, Universiti Tunku Abdul Rahman, Jalan Universiti, Bandar Barat, Kampar, Perak 31900, Malaysia
*Corresponding author (e-mail: yamunam@utar.edu.my)

Waste heat energy from industrial operations can be recovered using phase change material (PCM) due to its ability to store thermal energy at phase transition temperature. However, disadvantage such as leakage of PCM that causes corrosion of industrial equipment hinders the potential of PCM being used in large-scale. In this study, form-stable PCM was developed using polyamide/reduced graphene oxide(rGO) that was pelletised and coated with nitrile butadiene rubber (NBR) latex via dip coating method. Thermal cyclic analysis showed that the leakage of PCM has reduced as the sulphur loading in NBR latex increased. PCMs with two layers of NBR coating have lower weight loss compared to those with 1 layer of NBR coating especially at a higher sulphur loading. The Ultimate tensile strength (UTS) and E-modulus of the NBR films increased with sulphur loading due to an increase in crosslink density as indicated by gel fraction studies. The percentage of elongation at break (EB%) decreased as the crosslink density increased, due to restricted mobility of NBR chains. The increase in crosslink density has resulted in increase in gel fraction and density of the NBR films which then leads to formation of compact and continuous NBR coating film on PCM surface as evidenced from microscopy images and functional group analysis.

Keywords: Waste heat; PCM; leakage; thermal cyclic analysis; NBR latex

Received: December 2022; Accepted: March 2023

Waste heat is energy that is not used and is emitted into the environment from a process or equipment. Industrial waste heat is energy discharged into the environment from industrial processes via thermal carrier mediums such as flue gases and steam, resulting in thermal pollution to environment. The industrial sector accounts for one-third of global energy use, with up to half of it being lost as heat [1]. Recovery of waste heat is an efficient method of re-purposing waste energy to produce beneficial energy products [2]. The recovered waste heat could be used to heat cold water or air which could be used in industrial processes such as drying and fuel air mixer. The waste heat can also be used to generate electricity through power cycle [3]. Heat energy recovery can save a substantial amount of primary energy while also lowering greenhouse gas emissions. Recovered energy could be used on the same industrial site or transferred to adjacent facilities or heat distribution networks [4].

Thermal energy storage (TES) is a storage system which is able to store thermal energy by heating or cooling a storage medium in order to subsequently utilise the stored energy to heat and cool applications, and power generation [5]. TES is capable of eliminating the mismatch between energy supply and demand [6]. One of the most commonly used TES systems is latent heat storage (LHS) which uses phase transition temperature of material to store heat. In LHS, heat is stored in the materials as latent heat and polymeric based phase change materials (PCMs) are among the most popular material used for this purpose[7]. Among the many benefits of using PCMs for heat storage are their high thermal absorption density, consistent temperature control, compact size, evident energy-saving benefits, and a simple yet dependable construction [8]. Due to these inherent characteristics of PCM, the application of PCM has been found to be suitable for both domestic and industrial usage. The possible applications of PCMs are in the automobile industry, textile industry, air-conditioning system, waste heat recovery, solar thermal energy storage, cooling of electronic devices, and building energy conservation [9]–[15].

However, drawbacks such as large volume expansion during phase transition which leads to leakage and loss of material, and corrosion to industrial equipment often impedes the large-scale applications of PCM. Various research has been

†Paper presented at Rubbercon2022

conducted using methods such as impregnation, encapsulation, and blending with polymer in order to overcome these issues. Ramakrishnan et al. developed a form-stable PCM by using hydrophobic expanded perlite as the supporting material and had compared its performance with expanded perlite. Paraffin was vacuum impregnated into the hydrophobic expanded perlite and expanded perlite in order to compare the stability between the two form-stable PCMs. It was found that paraffin impregnated into expanded perlite showed a 48% leakage compared to paraffin impregnated into hydrophobic expanded perlite that showed minimum to no leakage when integrated into concrete mixture [16]. Sagara et al. had attempted to improve the thermal endurance of PCM through vacuum impregnation. D-mannitol was used as PCM and porous SiO_2 grains was used as the supporting material. It was observed that the PCM was thermally stable with no leakage after 5 thermal cycles [17]. PCMs encapsulated with protective shell materials has been vastly researched and has been proven to prevent the leakage of PCMs [18]. Another study conducted by Shi et al. using acetylated cellulose nanofibril (AcCNF) as encapsulating material to encapsulate paraffin PCM to produce shape stabilised PCM showed that higher percentage of AcCNF resulted in minimum to zero leakage as compared to lower percentage of AcCNF [19]. Aludin et al. conducted a study by blending paraffin PCM into polycaprolactone (PCL) with different weight percentage composition to produce a form-stable PCM. This study showed that blending the paraffin into polymer such as PCL could prevent the leakage problem related to pure paraffin PCM. The composition ratio of paraffin/PCL at 40/60 showed the least leakage whilst maintaining the shape of the PCM [20]. Sarcinella et al. had developed a form-stable PCM using polyethylene glycol (PEG) impregnated into porous Lecce stone granules. The study showed that there were minimal to zero leakage in impregnated PCM [21].

Graphene is a single carbon layer of graphite structure and reduced graphene oxide (rGO) is graphene oxide (GO) that has undergone chemical, thermal, or electrical processes to reduce oxygen content. rGO has gained popularity among researchers due to its exceptional mechanical, electrical, thermal, and barrier properties [22]. The incorporation of rGO to enhance the thermal conductivity of PCM have been extensively investigated over the years [23]. Ren, Cao, and Zhang [23] reported that the thermal conductivity of rGO/expanded graphite (rGO/EG) aerogel PCM had increased 4 times (0.79 W/mK) compared to that of pure paraffin (0.20 W/mK) when the mass ratio of EG was 6.06%. Han et al., had produced novel SiO2/ expandable graphite (EG)/paraffin composite PCMs. Paraffin was hold by nano SiO2 and porous EG. It could maintain its original shape with non-flowing condition up to 200˚C. The thermal conductivity of paraffin was 0.303 W/(mK) and improved up to 0.739 W/(mK) with addition of EG [24].

In this study, polyamide/reduced graphene oxide (rGO) was pelletised and coated with compounded nitrile butadiene rubber (NBR) latex subsequently vulcanized. The crosslink chemistry of the NBR latex was manipulated through the concentration of sulphur. The main aim is to produce a form-stable PCM with minimal to no leakage and reduced volume expansion. Leakage of PCM hinders industrial-scale applications in TES as it could cause major contamination or device failure in packaging and electronic equipment [25], [26]. The form-stable PCMs produced from this work aimed to be used for LHS in high temperature applications. NBR is chosen as coating material because the properties could be tailored using crosslinks and it exhibit high chemical resistance due to acrylonitrile content[27], [28]. Leakage percentage, tensile properties, gel fraction, density, crosslink chemistry and the surface morphology were determined in this study.

EXPERIMENTAL

Chemicals and Materials

Hexamethylenediamine (HMDA) was provided by Merck KGaA, Darmstadt, Germany, and Sebacoyl Chloride (92%) was acquired from Acros Organics, Selangor, Malaysia. N-hexane was supplied by Chemiz (M) Sdn. Bhd. while sodium dodecyl sulphate was provided by Sigma Aldrich Selangor, Malaysia. Reduced graphene oxide (rGO) was acquired from GO Advanced Solutions Sdn. Bhd., Selangor, Malaysia. Nitrile butadiene rubber (NBR) latex (total solid content of 65%), zinc 2-mercaptobenzothiazole (ZMBT), zinc diethyldithiocarbamate (ZDEC), zinc oxide (ZnO), sulphur, potassium hydroxide (KOH) was acquired from Zarm Scientific & Supplies Sdn.Bhd., Penang, Malaysia.

Preparation of PCM

The PCM was prepared through condensation polymerisation. 3g of HMDA and 3mL of sebacoyl chloride were added to 97 mL of water and 97mL of n-hexane respectively. 0.3 g of sodium dodecyl sulphate was added to the HMDA solution. 0.5 wt% of rGO was added to the aqueous mixture of HMDA and ultrasonicated until the solution was homogenized using Q500 Sonicator supplied by QSonica Sonicators, USA (500W and 20 kHz) with specifications of 30% tip, 59s on and 10s off. The sebacoyl chloride/n-hexane solution was then added slowly and carefully to aqueous mixture of HMDA solution so as to not to disturb the interface between the two solutions. The surface polymerization was carried out at the interface. The PCM was then washed with distilled water and dried in the oven (UN110, Memmert GmbH + Co. KG, Schwabach, Germany) for 48h at the temperature of 80°C. The dried sample was ground into powder and then pressed into pellets using tablet presser. Diameter and thickness of the pellet are 13 mm and 4.4 mm, respectively.

$$n\ \mathrm{ClCO}(CH_2)_8\mathrm{COCl} + n\ H_2\mathrm{N}(CH_2)_6NH_2 \rightarrow -[\mathrm{CO}(CH_2)_8\mathrm{CO} - \mathrm{NH}(CH_2)_6\mathrm{NH}]-_n + 2\ \mathrm{HCl}$$

Sebacoyl chloride *HMDA* *Polyamide 6,10*

Table 1. Formulation for compounding of NBR latex.

Item	TSC	PHR
NBR	67.97	100
ZnO	49.86	1.0
ZDEC	57.74	1.0
ZMBT	55.34	0.5
KOH	10	1.0
Sulphur	62.18	0, 0.5, 1.0, 1.5, 2.0

Compounding of NBR latex

NBR latex, ZnO, ZDEC, ZMBT, KOH, and sulphur were weighed. NBR was stirred with half the amount of KOH for 5 minutes at 350 rpm using an overhead stirrer (IKA Overhead Stirrers RW 20 Digital, Germany). ZnO, ZDEC, ZMBT, sulphur, and remaining KOH were then added to the NBR and was stirred for 30 minutes at 350 rpm. The sulphur loading was varied to study the effect of different sulphur concentration on the stability of PCMs. The compounded NBR were cast into films with a thickness of 0.5mm on a glass and cured in the oven at 150℃ for 20 minutes to determine the density of the films as well as to carry out tensile analysis and gel fraction. The formulation used for the compounding of NBR latex is tabulated in Table 1 below.

Coating of PCM

PCM pellets were dipped for 5 seconds into the compounded NBR latex using forceps. The dipped pellets were placed on a Teflon sheet and cured in the at 150℃ for 20 minutes. Pellets with 1 layer of NBR coating and 2 layers of NBR coating were prepared. The process was repeated for PCMs coated with 2 layers of NBR.

Thermal Cyclic Analysis

Thermal cyclic analysis was done on the coated PCMs to determine the leakage of the PCMs in terms of percentage of weight loss. The coated PCMs were heated to 235℃ on a hotplate for 3 minutes and cooled to room temperature repeatedly for 100 times. Thermal paste was used between the pellet and the hotplate to minimise air gaps and maximise heat transfer. The weight of coated PCMSs before and after 100 thermal cycles were recorded to calculate the percentage of weight loss. The calculation of percentage of weight loss is given by,

$$Weight\ loss\ (\%) = \frac{(W_0 - W_1)}{W_0} \times 100$$

where, W_0 = initial weight (g), W_1 = final weight (g).

Tensile Analysis

Tensile analysis of the compounded NBR latex films was carried out in accordance to the standard test method ASTM D412 to measure the E-modulus, tensile strength, and elongation at break. The tensile analysis was carried out using lightweight tensile tester, Model Tinius Olsen H10KS-0784 from Tinius Olsen Testing Machine Company supplied by Leader Technology Scientific Malaysia. The analysis was carried out with load of 450N, at a crosshead speed of 100 mm/min and gauge length of 26 mm. The films were cut into dumbbell shape using a dumbbell presser. Five tensile analyses were conducted for each film to obtain the average values.

Gel Fraction

Gel fraction is the fraction of the insoluble weight. It was obtained by extracting the soluble part of the NBR films in the Soxhlet extractor. The NBR films were cut into small pieces weighing 0.2 ± 0.05 g and folded into mesh wires. The NBR films were extracted in acetone solution at 80℃ for 24 hours. After extraction, the films were dried at 60℃ for 72 hours. The final weight of the films was measured, and the gel fraction was calculated using the formula below,

$$Gel\ fraction\ (\%) = \frac{W_1}{W_0} \times 100$$

where W_0 = initial weight (g), W_1 = dry weight of the film after extraction (g).

Density

The density of the NBR films was measured using a precision balance with density determining kit, Series 360ES Semi-Micro Balance supplied by Precisa Gravimetric Ag, Dietikon, Switzerland.

Morphology study using Field Emission Scanning Electron Microscopy (FESEM)

The surface morphology of the coated PCM were captured at different magnification (500x and 5000x) and recorded using field emission scanning electron microscope, model JEOL JSM 6701F supplied by JEOL (Malaysia) Sdn. Bhd., Selangor, Malaysia. Each sample was placed on a disc using scope tape. To eliminate electrostatic charge and low image quality, all samples were inspected after being sputter coated with a thin layer of platinum.

Attenuated Total Reflectance (ATR-FTIR)

The FTIR analysis of the NBR latex films and coated PCMs after thermal cyclic analysis was examined using PerkinElmer Spectrum Two FTIR spectrometer through the ATR method. The scanning wavelength range was from 400 cm-1 to 4000 cm-1 at 32 scans.

RESULTS AND DISCUSSION

Thermal Cyclic Analysis

The weight loss percentage of the NBR coated PCMs were evaluated and are shown in Figure 1. NBR coated PCMs with 2 PHR of sulphur loading showed the least amount of weight lost. The overall results show reduction in percentage of weight lost as the sulphur loading increases. This is due to increase in crosslink density with increase in sulphur loading[29]. Sulphur is a vulcanizing agent that forms crosslinks between the carbon-carbon double bonds (C=C) in order to achieve a three-dimensional network [30]. As the loading of sulphur increases in the rubber, more sulphidic bonds are formed which results in higher tensile strength to withstand the pressure build-up due to phase change in the PCM and therefore reducing the weight lost in the PCM [31]. PCMs with two layers NBR coating have lower weight loss compared to those with 1 layer of NBR coating especially at a higher sulphur loading. This is because the 2 layers of NBR coatings encapsulates the PCMs more securely and thus minimising the weight lost of PCM. Higher sulphur loading combined with 2 layers of NBR results in lowest weight lost due to high crosslink density and more compact coating that prevents high amount of PCM from leaking out.

Tensile Analysis

The tensile properties such as the E-modulus, Ultimate Tensile Strength (UTS) and Elongation at Break (EB%) of the NBR films with different sulphur loading were analysed and tabulated in Table 1. UTS of the NBR is the stress it can withstand before it breaks. It can be observed that the UTS increases as the sulphur loading increases. At 2 PHR sulphur loading, the UTS was at 4.805 MPa compared to only 2.522 MPa at 0 PHR of sulphur loading. The UTS is proportional to the sulphur loading as the crosslink density increases with sulphur loading [32]. Increase in crosslink density caused by higher sulphur loading results in increase of sulphidic bonds that reduces the mobility of the NBR polymer chains [29]. E-modulus of the NBR is the stress needed to strain the samples to 100%. Results obtained show that the E-modulus increases with increase in sulphur loading, similar to the trend shown in UTS.

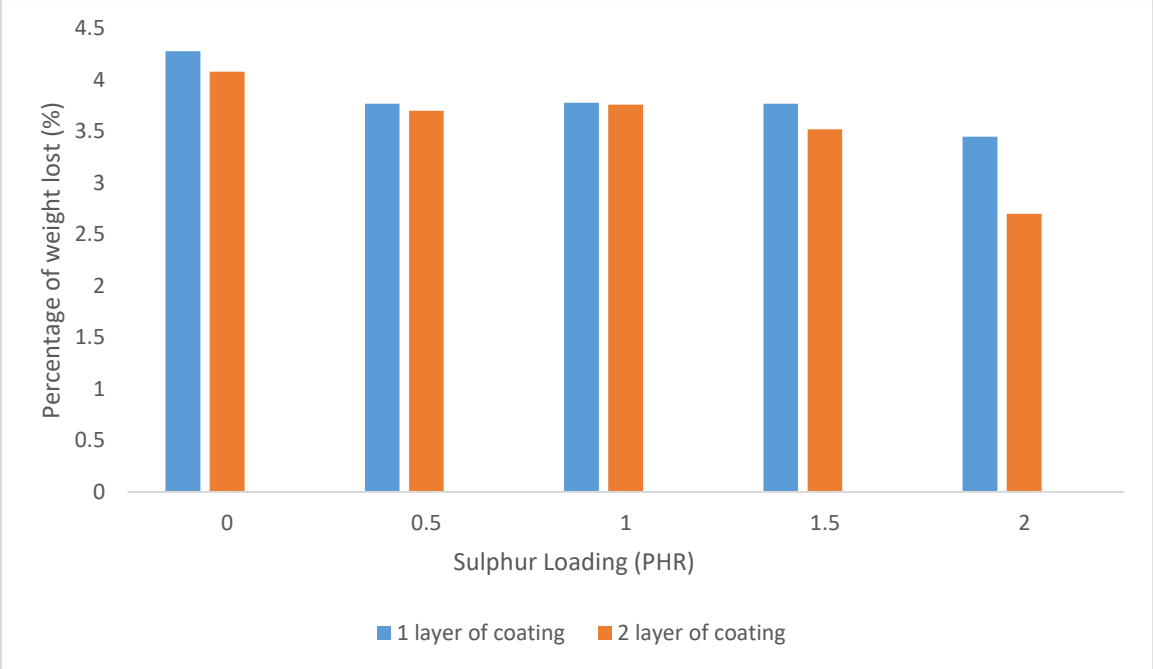

Figure 1. Thermal cyclic analysis results.

Table 2. Tensile analysis of NBR films with different Sulphur loading.

Sulphur Loading (PHR)	E-modulus (MPa)	Ultimate Tensile Strength (MPa)	Elongation at Break (%)
0	0.047 ± 0.0093	2.522 ± 0.737	1752 ± 207.7
0.5	1.068 ± 0.3362	2.748 ± 0.433	749 ± 139.5
1	1.209 ± 0.1346	2.953 ± 0.1217	480 ± 21.56
1.5	1.8 ± 0.537	3.088 ± 1.072	358.7 ± 132.4
2	1.915 ± 0.3269	4.805 ± 0.622	241.9 ± 175.7

It can be observed that EB% decreases as the sulphur loading increases. This is due to increase in crosslink density with increase in sulphur loading. EB% is the extent to which samples elongate before it breaks. At 0 PHR of sulphur, the EB% is at 1752% whereas at 2 PHR, it is at 241.9%. As the crosslinking density increases, the chain mobility reduces leading to less elastic NBR. When the coating films are less elastic, it will form cracks and fail easily[33].

Gel Fraction

The gel fraction results of the NBR films are shown in Table 2. The gel fraction of the NBR films were determined to measure the percentage of insoluble rubber in the films. Based on the results obtained, the gel fraction of the NBR films increases as the sulphur loading increases. At 2 PHR of sulphur, the gel fraction is the highest at 89.98%. The percentage of gel fraction that remains after Soxhlet extraction indicates the crosslink density of the NBR films as gel fraction is directly proportional to the crosslink density. The increase in gel fraction shows that there is an increase in crosslink density when sulphur loading increases from 0 PHR to 2 PHR. Results obtained show that the improvement in weight loss percentage with increase in sulphur loading in thermal cyclic test is due to increase in crosslink density which results in higher tensile strength to withstand pressure build-up caused by volume expansion during phase change [31], [34].

Density

Table 3 shows the density of the NBR films. Based on the results obtained, it can be observed that the density of the NBR has increased slightly as the sulphur loading increases. For example, the density of NBR film at 2 PHR is 0.973 g/cm^3, which is higher than the density of NBR at 0 PHR sulphur. This shows that as the crosslink density increases, a more compact chain structure is formed in the NBR films due to the three-dimensional crosslink network. The free volume between the chains will also decrease.

Table 3. Gel fraction of NBR films with different Sulphur loading.

Sulphur Loading (PHR)	Gel Fraction (%)
0	70.57
0.5	83.08
1	83.71
1.5	88.44
2	89.98

Table 4. Density of NBR films with different sulphur loadings.

Sulphur Loading (PHR)	Density (g/cm^3)
0	0.929
0.5	0.942
1	0.946
1.5	0.956
2	0.973

Morphology Study

Figure 2 a) shows that uncoated PCM are fibrous, rough, and uneven, the coated PCMs show flat and smoother surfaces. Figure 2 b) shows that with 2 layers of NBR coating at 2 PHR sulphur loading, the coating layer is smooth and has minimal to no cracks and holes, thus, verifying that the high crosslink density reduces the leakage of the PCM. At lower sulphur loading, as shown in Figure 2c), there are some cracks formed. Figure 2d) shows the most cracks in the coating, confirming that the high amount of leakage in thermal cyclic test of single layer NBR coated PCMs is due to discontinuous coating.

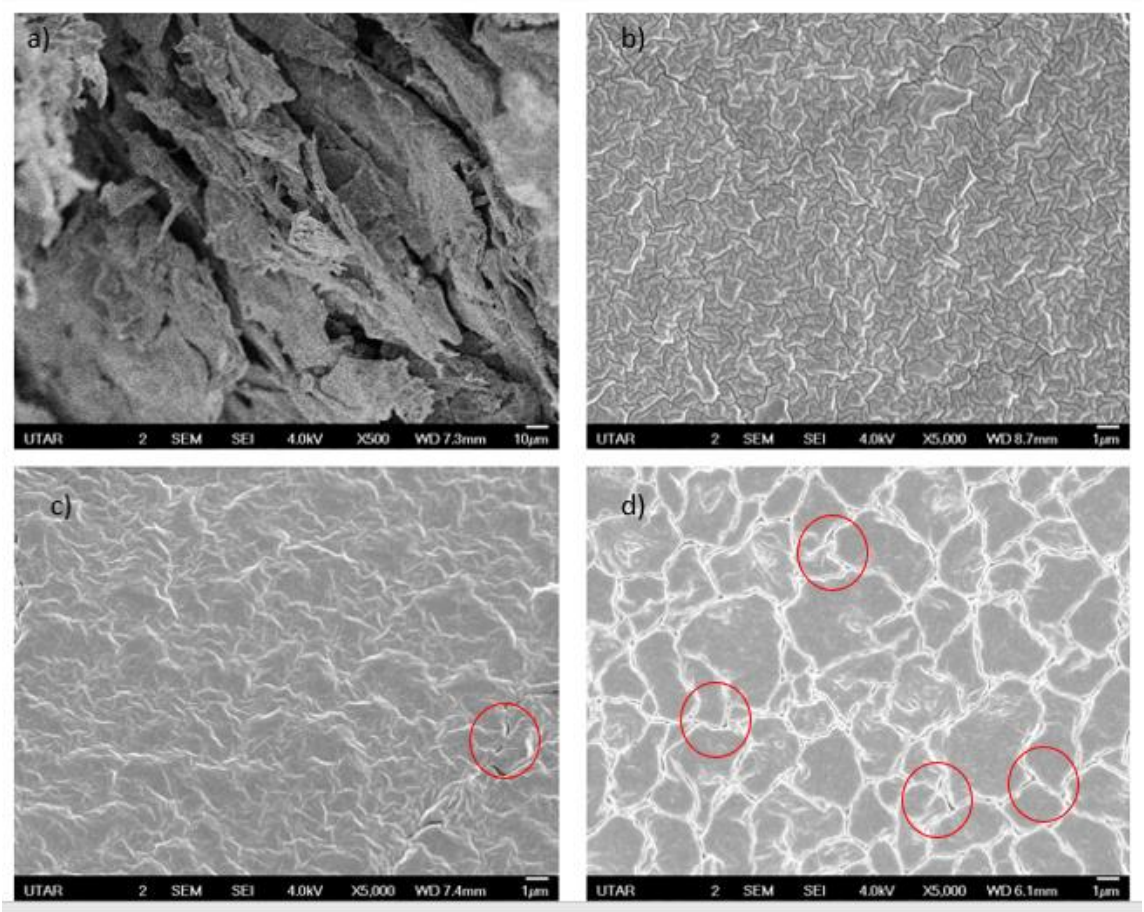

Figure 2. FESEM images of PCMs a) before NBR coating; b) 2 layers of NBR coating with 2 PHR sulphur; c) 2 layers NBR coating with 1.5 PHR sulphur; and d) 1 layer of NBR coating with 1.5 PHR sulphur.

ATR-FTIR

Figures 3 shows the ATR-FTIR results of coated PCM and figure 4 shows the ATR-FTIR of NBR filmsat 2 PHR and 0 PHR of sulphur loadings, respectively. Based on the results obtained, coated PCM and the NBR films have similar peaks, showing good coverage of NBR coating on the PCM. As it can be observed in both Figures 3 and 4, there are peaks associated with O-H symmetric vibrations at 3429 cm^{-1}, 3422 cm^{-1}, and 3429 cm^{-1}. Peaks at 2922 cm^{-1} and 2853 cm^{-1} belong to C-H vibrations [35]. Stretching of C-N group in NBR at the peak 2237 cm^{-1} and 2238 cm^{-1} could be observed [36]. The peaks at 1550 cm^{-1} -1592 cm^{-1} are associated with the chemical bond of -C=C- and the peak at 970 cm^{-1} is associated with -CH=CH (trans) bond [37].

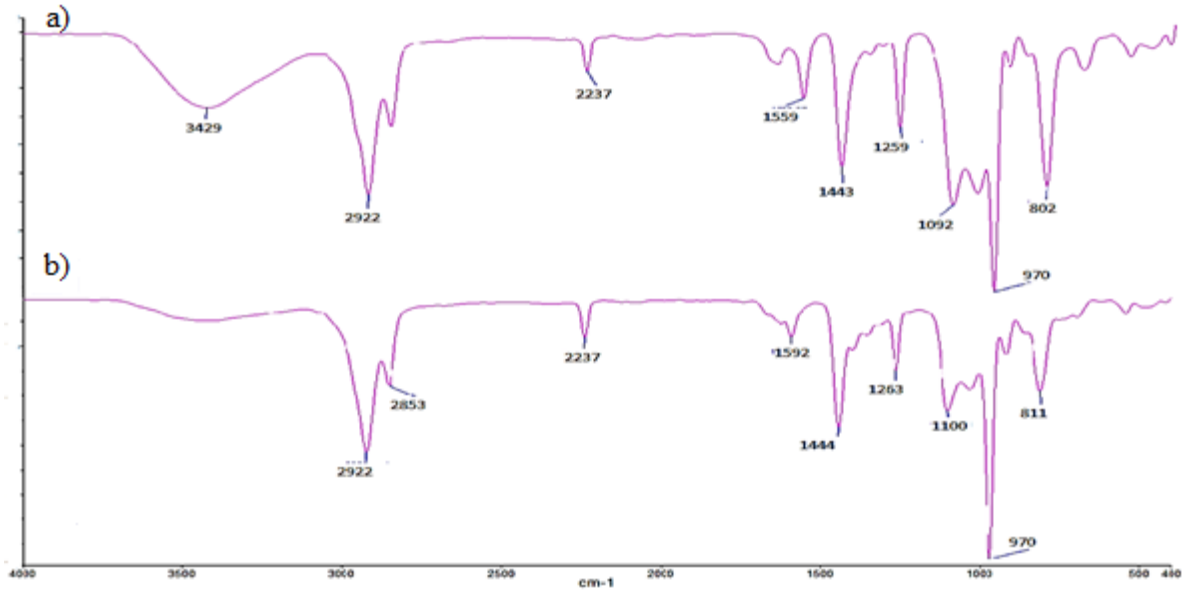

Figure 3. ATR-FTIR of PCMs coated with a) 2 layers of NBR at 2PHR sulphur and b) 1 layer of NBR at 0 PHR sulphur.

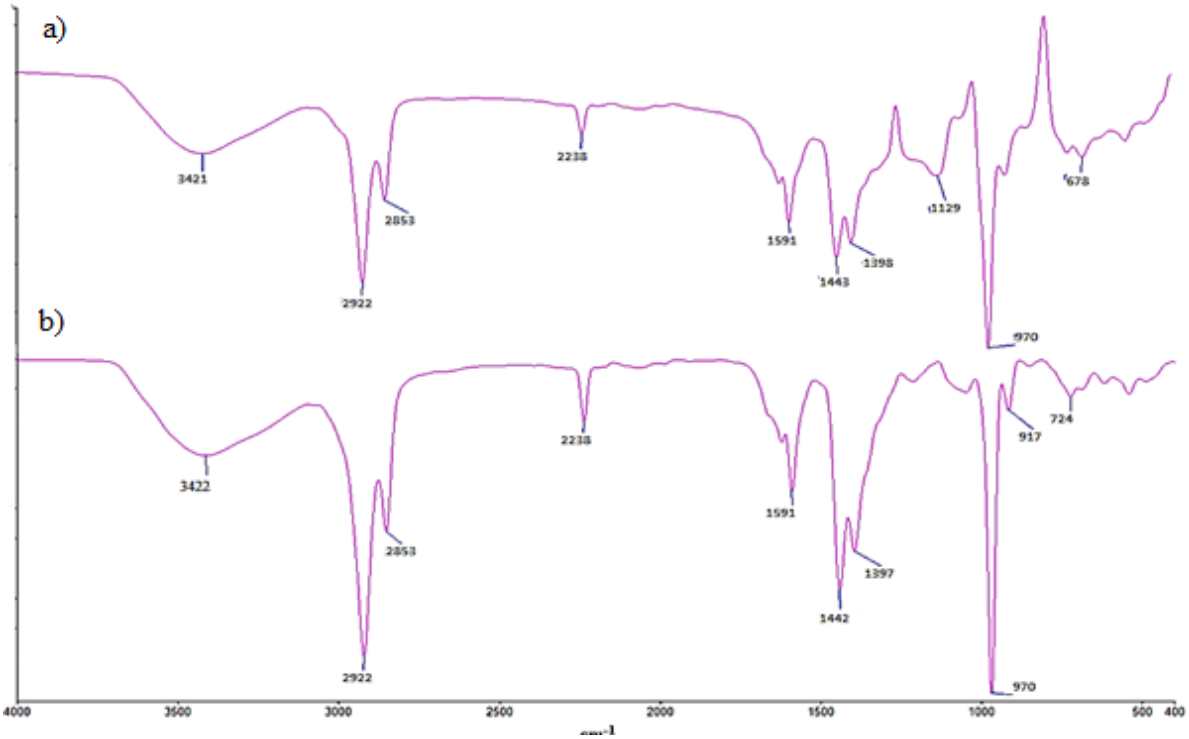

Figure 4. ATR-FTIR of NBR film with a) 2 PHR sulphur and b) NBR film with 0 PHR sulphur.

CONCLUSION

In this work, form-stable PCMs were produced by coating polyamide/reduced graphene oxide(rGO) based PCM with vulcanized NBR. The PCM was developed polyamide/reduced graphene oxide(rGO) was synthesised using condensation polymerisation method using the surface technique. The weight loss percentage of the NBR coated PCMs show that there is reduction in percentage of weight lost as the sulphur loading increases due to increase in crosslink density. As the loading of sulphur increases in the rubber, more sulphidic bonds are formed thus resulting in lower leakage percentage. PCMs with two layers NBR coating showed lower weight loss compared to those with 1 layer of NBR coating.

Tensile analysis show that the UTS and E-modulus of NBR with 2 PHR were the highest at 4.805 MPa and 1.915 MPa, respectively. Gel fraction of the NBR films increases as the sulphur loading increases. The density of the NBR films showed a slight increase in trend with the increase in sulphur loading due to formation of more compact chain structure in the NBR. The coated PCM with 2 layers of NBR coating at 2 PHR sulphur showed a smooth coating with minimal to no cracks and holes, proving that the sulphur loading reduces leakage of PCM. ATR-FTIR showed that the coated PCMs have similar peaks with NBR films, showing good coverage of NBR coating on the PCMs. Based on the results obtained, the PCM coated with 2 layers NBR at 2 PHR sulphur showed the least leakage, highest UTS and E-modulus, making it the most suitable form-stable PCM to be used in industry for waste heat recovery.

ACKNOWLEDGEMENTS

This research was funded by Universiti Tunku Abdul Rahman Research Fund, grant number 6220/P17.

REFERENCES

1. Woolley, E., Luo, Y. and Simeone, A. (2018) Industrial waste heat recovery: A systematic approach. *Sustainable Energy Technologies and Assessments*, **29**, 50–59, Oct. 2018. doi: 10.1016/J.Seta.2018.07.001.

2. Loni, R., Najafi, G., Bellos, E., Rajaee, F., Said, Z. and Mazlan, M. (2021) A review of industrial waste heat recovery system for power generation with Organic Rankine Cycle: Recent challenges and future outlook. *J Clean Prod*, **287**, Mar. 2021. doi: 10.1016/J.Jclepro.2020.125070.

3. Arabkoohsar, A. (2020) Combination of air-based high-temperature heat and power storage system with an Organic Rankine Cycle for an improved electricity efficiency. *Appl Therm Eng*, **167**, Feb. 2020. doi: 10.1016/J.Applthermaleng.2019.114762.

4. Bianchi, G., et al. (2019) Estimating the waste heat recovery in the European Union Industry. *Energy, Ecology and Environment*, **4**, 5, 211–221, Sep. 2019. doi: 10.1007/S40974-019-00132-7.

5. Sarbu, I. and Sebarchievici, C. (2017) Thermal Energy Storage. *Solar Heating and Cooling Systems*, 99–138. doi: 10.1016/B978-0-12-811662-3.00004-9.

6. Pfleger, N., Bauer, T., Martin, C., Eck, M. and Wörner, A. (2015) Thermal energy storage - overview and specific insight into nitrate salts for sensible and latent heat storage. *Beilstein Journal of Nanotechnology*, **6**, 1, 1487–1497. doi: 10.3762/Bjnano.6.154.

7. Hailu, G. (2021) Energy systems in buildings in *Energy Services Fundamentals and Financing*, Elsevier, 181–209. doi: 10.1016/B978-0-12-820592-1.00008-7.

8. Wang, Z. (2019) Thermal Storage Systems. *Design of Solar Thermal Power Plants*, 387–415. doi: 10.1016/B978-0-12-815613-1.00006-7.

9. Vakhshouri, A. R. (2020) Paraffin as Phase Change Material in *Paraffin - an Overview*, IntechOpen. doi: 10.5772/intechopen.90487.

10. Saeed, R. M. R. (2016) Thermal characterization of phase change materials for thermal energy storage energy storage. Masters Thesis, Missouri University of Science and Technology.

11. Zhou, D., Zhou, Y., Liu, Y., Luo, X. and Yuan, J. (2019) Preparation and Performance of Capric-Myristic Acid Binary Eutectic Mixtures for Latent Heat Thermal Energy Storages. *J Nanomater*, Aug. 2019. doi: 10.1155/2019/2094767.

12. Sundararajan, S., Samui, A. B. and Kulkarni, P. S. (2017) Versatility of polyethylene glycol (PEG) in designing solid–solid phase change materials (PCMs) for thermal management and their application to innovative technologies. *J Mater Chem A Mater*, **5**, 35, 18379–18396. doi: 10.1039/C7TA04968D.

13. Kraft, W. and Altstedde, M. K. (2016) Use of metallic Phase Change Materials (mPCM) for heat storage in Electric- and Hybrid Vehicles in *6th Hybrid and Electric Vehicles Conference (HEVC 2016)*. doi: 10.1049/cp.2016.0974.

14. Sharma, R. K., Ganesan, P., Tyagi, V. V., Metselaar, H. S. C. and Sandaran, S. C. (2015) Developments in organic solid–liquid phase change materials and their applications in thermal energy storage. *Energy Convers Manag*, **95**, 193–228, May 2015. doi: 10.1016/j.enconman.2015.01.084.

15. Zalba, B., Marín, J. M., Cabeza, L. F. and Mehling, H. (2003) Review on thermal energy storage with phase change: Materials, heat transfer analysis and applications. *Applied Thermal Engineering*, **23**, 3, 251–283, Feb. 2003. doi: 10.1016/S1359-4311(02)00192-8.

16. Ramakrishnan, S., Sanjayan, J., Wang, X., Alam, M. and Wilson, J. (2015) A novel paraffin/ expanded perlite composite phase change material for prevention of PCM leakage in cementitious composites. *Appl Energy*, **157**, 85–94, Nov. 2015. doi: 10.1016/J.Apenergy.2015.08.019.

17. Sagara, A., Nomura, T., Tsubota, M., Okinaka, N. and Akiyama, T. (2014) Improvement in thermal endurance of D-mannitol as phase-change material by impregnation into nanosized pores. *Mater Chem Phys*, **146**, 3, 253–260, Aug. 2014. doi: 10.1016/ J.Matchemphys.2014.03.009.

18. Alva, G., Lin, Y., Liu, L. and Fang, G. (2017) Synthesis, characterization and applications of microencapsulated phase change materials in thermal energy storage: A review. *Energy Build*, **144**, 276–294, Jun. 2017. doi: 10.1016/J.Enbuild. 2017.03.063.

19. Shi, X., Yazdani, M. R., Ajdary, R. and Rojas, O. J. (2021) Leakage-proof microencapsulation of phase change materials by emulsification with acetylated cellulose nanofibrils. *Carbohydr Polym*, **254**, 117279, Feb. 2021. doi: 10.1016/J.Carbpol. 2020.117279.

20. Aludin, M. S. and Saidatul Akmal, S. (2017) Preparation and characterization of form-stable paraffin/polycaprolactone composites as phase change materials for thermal energy storage. *MATEC Web of Conferences*, **97**, 01094, Feb. 2017. doi: 10.1051/Matecconf/20179701094.

21. Sarcinella, A., de Aguiar, J. L. B. and Frigione, M. (2022) Physical Properties of an Eco-Sustainable, Form-Stable Phase Change Material Included in Aerial-Lime-Based Mortar Intended for Different Climates. *Materials*, **15**, 1192, Feb. 2022. doi: 10.3390/MA15031192.

22. Smith, A. T., LaChance, A. M., Zeng, S., Liu, B. and Sun, L. (2019) Synthesis, properties, and applications of graphene oxide/reduced graphene oxide and their nanocomposites. *Nano Materials Science*, **1**, 1, 31–47, Mar. 2019, doi: 10.1016/ J.Nanoms.2019.02.004.

23. Ren, W., Cao, L. and Zhang, D. (2020) Composite phase change material based on reduced graphene oxide/expanded graphite aerogel with improved thermal properties and shape-stability. *Int J Energy Res.*, **44**, 1, 242–256, Jan. 2020. doi: 10.1002/ER.4900.

24. Han, X., Zhao, T., Gao, X. and Li, H. (2018) Preparation and characterization of high-temperature non-flowing SiO2/EG/paraffin composites by high-temperature refining. *Colloids Surf A Physicochem Eng Asp*, **542**, 1–7, Apr. 2018. doi: 10.1016/J. Colsurfa.2018.01.043.

25. Zhang, Q., Liu, J., Zhang, J., Lin, L. and Shi, J. (2022) A Review of Composite Phase Change Materials Based on Biomass Materials. *Polymers*, **14**, 19, 4089, Sep. 2022. doi: 10.3390/Polym 14194089.

26. Umair, M. M., Zhang, Y., Iqbal, K., Zhang, S. and Tang, B. (2019) Novel strategies and supporting materials applied to shape-stabilize organic phase change materials for thermal energy storage–A review. *Appl Energy*, **235**, 846–873, Feb. 2019. doi: 10.1016/J.Apenergy.2018.11.017.

27. Cai, Z., Li, Y., Yang, Z. and Jiang, M. (2020) Effects of acrylonitrile content of nitrile rubber on mechanical properties of polyamide 6/nitrile rubber blends. *Mater Res Express*, **6**, 12, 125362, Jan. 2020. doi: 10.1088/2053-1591/AB612A.

28. Lenko, D., Schlögl, S., Temel, A., Schaller, R., Holzner, A. and Kern, W. (2013) Dual cross-linking of carboxylated nitrile butadiene rubber latex employing the thiol-ene photoreaction. *J Appl Polym Sci*, **129**, 5, 2735–2743, Sep. 2013. doi: 10.1002/APP.38983.

29. Alshabatat, N. and Abouel-Kasem, A. (2021) The Effects of Sulfur Content on the Mechanical Properties of Nitrile Butadiene Rubber with Different Aging Conditions. *Jordan Journal of Mechanical and Industrial Engineering*, **15**, 4.

30. Woolfson, A. D., Malcolm, R. K., Gorman, S. P. and Mccullagh, S. D. (2009) Self-lubricating catheter materials. *Biomaterials and Tissue Engineering in Urology*, 191–207, Jan. 2009. doi: 10.1533/9781845696375.2.191.

31. Bin Samsuri, A. and Abdullahi, A. A. (2017) Degradation of Natural Rubber and Synthetic Elastomers. *Reference Module in Materials Science and Materials Engineering*, Jan. 2017. doi: 10.1016/B978-0-12-803581-8.09212-2.

32. Bakhshandeh, G. R., Farahani, T. D. and Emamikia, M. (2008) Effect of curing system on mechanical properties of NBR/nylon-PET cord composite. *E-Polymers*, Feb. 2008. doi: 10.1515/Epoly. 2008. 8.1.273.

33. Cichomski, E., et al. Effect of the crosslink density and sulfur-length on wet-traction and

rolling resistance performance indicators for passenger car tire tread materials.

34. Kim, J. -H., Choi, K. -C., Yoon, J. -M. and Kim, S. -Y. (2009) Cure characteristics and physical properties of hydrogenated acrylonitrile butadiene rubber: Effects of prevulcanization temperature and time. *Journal of Industrial and Engineering Chemistry*, **12**, 4, 608–614, Mar. 2009.

35. Zhao, J., Yang, R., Iervolino, R. and Barbera, S. (2013) Changes of Chemical Structure and Mechanical Property Levels during Thermo-Oxidative Aging of NBR. *Rubber Chemistry and Technology*, **86**, 4, 591–603, Dec. 2013. doi: 10.5254/RCT.13.87969.

36. Sanches, N. B., Pedro, R., Diniz, M. F., Mattos, E. da C., Cassu, S. N. and Dutra, R. de C. L. (2013) Infrared spectroscopy applied to materials used as thermal insulation and coatings. *Journal of Aerospace Technology and Management*, **5**, 4, 421–430. doi: 10.5028/JATM.V5I4.265.

37. Sadeghalvaad, M., Dabiri, E., Zahmatkesh, S. and Afsharimoghadam, P. (2018) Preparation and properties evaluation of nitrile rubber nanocomposites reinforced with organo-clay, CaCO3, and SiO2 nanofillers. *Polymer Bulletin*, **76**, 8, 3819–3839, Oct. 2018. doi: 10.1007/S00289-018-2583-8.